JOURNAL OF AIRCRAFT
Vol. 44, No. 3, May–June 2007

Automatic Transition Prediction and Application to Three-Dimensional High-Lift Configurations

Andreas Krumbein*
DLR, German Aerospace Center, 37073 Göttingen, Germany

DOI: 10.2514/1.25528

A Reynolds-averaged Navier–Stokes solver, a laminar boundary-layer code and two e^N-database methods for the prediction of transition due to Tollmien–Schlichting and crossflow instabilities were coupled to be applied to 3-D high-lift aircraft configurations which are of industrial relevance. The first application of the coupled system to a wing-body configuration with a three-element wing consisting of slat, main wing, and flap is described and documented in this paper. The prediction of the laminar–turbulent transition lines was done in a fully automatic manner. It will be shown that complex aircraft configurations can be handled without a priori knowledge of the transition characteristics of the specific flow problem. The computational results are compared with experimental data.

Nomenclature

b	=	semispan
c	=	local chord length
c_p	=	pressure coefficient
k_{cyc}	=	number of RANS cycles for the transition location iteration, which represents the interval between two calls of the transition prediction module
n_T	=	global number of transition points
Tu	=	turbulence intensity
x	=	longitudinal coordinate of the configuration in the global coordinate system of the RANS solver
x^T	=	longitudinal coordinate value of the transition point
z	=	spanwise coordinate being perpendicular to the longitudinal axis
α	=	angle of attack
γ	=	value of the intermittency
δ_F	=	flap deflection angle
δ_S	=	slat deflection angle
η	=	nondimensional spanwise coordinate

Subscripts

CF	=	crossflow
crit	=	critical
j	=	counter of the transition points
TS	=	Tollmien–Schlichting
∞	=	freestream value

I. Introduction

THE modeling of laminar–turbulent transition in Reynolds-averaged Navier–Stokes (RANS) solvers is a necessary requirement for the computation of flows over airfoils and wings in the aerospace industry because it is not possible to obtain quantitatively correct results if the laminar–turbulent transition is not taken into account. Especially the simulation of flows around high-lift systems of aircraft may result in significant errors when the transition points are simply estimated or are not taken into account at all. High-lift systems very often involve multicomponent wings (e.g., slat, main wing, and flaps) and usually exhibit very high levels of total circulation. Because all components of the high-lift system are in close interaction with one another, the total circulation and the complete flowfield is affected by one transition line on one of the components.

Although the overall lift value may be predicted with satisfactory accuracy, slight deviations between the real and the computed pressures can lead to large errors in the computed overall drag value. This issue was investigated in detail in [1] and it was shown that the overall pressure drag of a high-lift configuration, which dominates the drag value of the configuration as a whole as well as the drag of every single element, is composed of a balance of very large positive and negative contributions. The contribution of one single element may be one order of magnitude larger than the resulting overall drag of the complete configuration. Thus, a relative error of 5% of the computed drag on the slat upper side may result in a change of 50% for the overall drag value. This effect occurs, for example, due to suction peaks at the noses of the wing elements that do not reach the desired high pressure levels at large angles of attack, so that the suction force is too low and leads to a change of the overall drag on the one hand. On the other hand, the location of separation and the extent of the separation region are sensitive to the location of the laminar–turbulent transition lines because separation depends on the upstream history of the boundary layer.

For the design process of aircraft high-lift systems in industry, there exists the demand for a RANS-based computational fluid dynamics (CFD) tool that is able to handle flows automatically and autonomously with laminar–turbulent transition. Existing transition prediction methods vary from empirical transition criteria via the local, linear stability equations based on small disturbance theory or nonlocal, linear and nonlocal, nonlinear stability methods using the parabolized stability equations over large eddy simulations to direct numerical simulations of the Navier–Stokes equations. Empirical transition criteria and the e^N method [2,3] based on local, linear stability theory and the parallel flow assumption represent *state-of-the-art* methods for the prediction of transition onset in many industrial applications. Although they do not account for a number of fundamental aspects in the transition process, e^N methods are used in aircraft industry most frequently for design purposes covering transition due to Tollmien–Schlichting and crossflow instabilities. Because there are no other practical methods presently available for industrial applications [4], e^N methods together with the two-N-factor method and empirical criteria for transition mechanisms that are not covered by the e^N approach (e.g., bypass and attachment line transition) are going to be used further on for the design of aircraft

Presented as Paper 3164 at the 24th Applied Aerodynamics Conference, San Francisco, 5–8 June 2006; received 12 June 2006; revision received 13 February 2007; accepted for publication 14 February 2007.

*Research Scientist, Research and Development Engineer, Institute of Aerodynamics and Flow Technology, Numerical Methods, Bunsenstraße 10; andreas.krumbein@dlr.de. Member AIAA.

wings and wing systems even for a future laminar wing of transport-type aircraft.

The first steps towards the setup of a RANS-based CFD tool with automatic transition prediction were made, for example, in [5], where a RANS solver and an e^N method were applied and in [6], where a RANS solver, a laminar boundary-layer method [7], and an e^N method were coupled. There, the boundary-layer method was used to produce highly accurate laminar, viscous layer data to be analyzed by a linear stability code. Hence, the very expensive grid adaptation necessary to produce accurate viscous layer data directly from a structured Navier–Stokes grid was avoided. The use of e^N-database methods [8,9] results in a coupled program system that is able to handle transition prediction automatically. In [10], a database for the growth rates is used, which are represented by a trained neural network based on Falkner–Skan–Cooke profiles. Alternative approaches using a transition closure model or a transition/turbulence model directly incorporated into the RANS solver are documented in [11–13]. A correlation-based transition modeling approach built on local variables using transport equations for the intermittency and for a transition onset criterion in terms of the momentum thickness Reynolds number is documented in [14].

At the German Aerospace Center (DLR), the block-structured RANS code FLOWer [15] is used together with the laminar boundary-layer method in [7] and the e^N-database methods in [8,9]. The laminar boundary-layer method and the e^N-database methods form a so-called transition prediction module that is coupled to the RANS solver and that interacts with the RANS solver during the computation [16,17]. Presently, the transition prediction module of the FLOWer code can be applied to 2-D one-element or multielement configurations and to 3-D one-element or multielement wing configurations.

In [18–20], the FLOWer code was applied to 2-D multielement airfoil configurations and 3-D one-element wing configurations with transition. In the present paper the first application to 3-D high-lift configurations is documented. The main objective is to show that the coupling structure between a RANS solver and the transition prediction module can be applied to 3-D high-lift flows over wings of transport type aircraft in an automatic manner, and in the same way as it was done before for 2-D airfoil flows and 3-D one-element wing flows, and that the FLOWer code provides all technical features that are necessary for the transition prediction on industrially relevant aircraft configurations. The first results of the current version of the transition prediction module for a 3-D high-lift system of an aircraft are presented and discussed as well as the results from the RANS computations carried out. The differences between the computational results for fully turbulent flow, flow with prescribed transition locations, and flow with predicted transition locations are outlined. In all computations with transition, "point transition" was applied; that is, no transitional flow models were used. The computed results are compared with experimental findings.

The work presented in this paper is of preliminary character with regard to the conclusiveness of the predicted transition locations, because typical transition mechanisms that can cause transition in 3-D flows, such as transition inside laminar separation bubbles or attachment line transition, are not yet covered by the transition prediction module. Also, bypass transition, which may play a role when a wing component, for example, the flap, is located in the wake of an upstream located wing element can play a role. The incorporation of empirical criteria for these transition mechanisms as well as the incorporation of a fully automated linear stability code that can replace the e^N-database methods will be done in the near future.

II. Transition Prediction Coupling Structure

The FLOWer code [15] is a 3-D, compressible RANS code for steady or unsteady flow problems and uses structured body-fitted multiblock meshes. The code is based on a finite volume formulation and provides a cell vertex as well as a cell-centered spatial discretization scheme using central differencing. Dissipative terms are explicitly added to damp high-frequency oscillations and to achieve a sufficiently sharp resolution of shockwaves. The dissipative operator comprises second-order ($k^{(2)}$) and fourth-order ($k^{(4)}$) differences scaled by the largest eigenvalue following Jameson et al. [21] and Martinelli and Jameson [22]. On smooth meshes, the scheme is second-order accurate in space. The time integration is carried out using an explicit hybrid multistage Runge–Kutta scheme. For steady-state calculations, the integration is accelerated by local time stepping and implicit residual smoothing. These techniques are embedded in a multigrid algorithm. The code allows two dummy cells around each block to maintain second-order accuracy in space at block intersections. The influence of turbulence is taken into account either by eddy viscosity turbulence models according to the Boussinesq approximation or by algebraic or differential Reynolds stress models. The transition handling is independent of the block topology of the computational grid and of the grid structure (structured, unstructured, or hybrid grid) [16].

The transition prediction module coupled to the FLOWer code consists of a laminar boundary-layer method for swept, tapered wings [7] and different transition prediction methods, which are provided with all necessary boundary-layer data by the laminar boundary-layer method. The laminar boundary-layer method solves the compressible laminar boundary-layer equations for conical external flow. Besides a number of empirical transition criteria, the most general transition prediction methods that are currently available are an e^N-database method for Tollmien–Schlichting (TS) instabilities [8] and an e^N-database method for crossflow (CF) instabilities [9].

The RANS solver communicates the surface pressure distribution of the configuration as input data to the laminar boundary-layer method, the laminar boundary-layer method computes all of the boundary-layer parameters that are needed for the transition prediction methods, and the transition prediction methods determine new transition locations that are given back to the RANS solver.

This coupling structure results in an iteration procedure for the transition locations within the iteration of the RANS equations. The structure of the approach is outlined graphically in Fig. 1.

During the computation, the RANS solver is stopped after a certain number of iteration cycles, k_{cyc}, usually when the lift has sufficiently converged, that is, when pressure oscillations have been damped to a sufficiently low degree. Then, the transition module is called and first the surface pressure distribution $c_p(\text{cycle} = k_{\text{cyc}})$ along a wing section is used as input for the boundary-layer code. All viscous data, basically the velocity profiles in streamwise and crossflow direction and their first and second derivatives, are calculated by the boundary-layer code. Then, the two e^N-database methods analyze the laminar boundary layer and try to determine a transition point that is located upstream of the separation point predicted by the boundary-layer code. If a transition point due to TS or CF instabilities was found, it is communicated back to the RANS solver. If no transition point due to TS or CF instabilities upstream of the laminar separation point could be found, the laminar separation point is used as approximation of the real transition point. This is an attempt to predict transition due strictly to the presence of separation bubbles. This approach often yields a good approximation of the real transition point when transition does not occur before the laminar boundary layer separates, particularly for low Reynolds number flows. These steps are done for the upper and lower sides of all specified wing sections. When all new transition locations, $x_j^T(\text{cycle} = k_{\text{cyc}})$ with $j = 1, \ldots, n_T$, where n_T is the number of

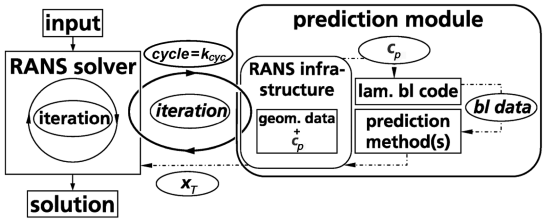

Fig. 1 Coupling structure of the RANS solver and the transition prediction module.

Table 1 Full span transition locations for the computation with prescribed transition

Element	$\alpha = 10.0$ deg		$\alpha = 14.0$ deg	
	Upper side	Lower side	Upper side	Lower side
Slat	$(x^T/c)^{\text{slat}} = 0.21$	At trailing edge	$(x^T/c)^{\text{slat}} = 0.11$	At trailing edge
Main	$(x^T/c)^{\text{main}} = 0.08$	At trailing edge	$(x^T/c)^{\text{main}} = 0.05$	$(x^T/c)^{\text{main}} = 0.15$
Flap	Beneath main	At trailing edge	Beneath main	At trailing edge

transition points, have been communicated back to the RANS solver, each transition location is slightly underrelaxed to damp oscillations in the convergence history of the transition locations. Then, all underrelaxed transition points (they represent a transition line on the upper or lower surface of a wing element in form of a polygonial line) are mapped into the surface grid of the configuration applying a transition setting algorithm [16,17] subdividing the surface of the geometry into laminar and turbulent regions, and the computation is continued. In so doing, the determination of the transition locations becomes an iteration process itself. With each transition location iteration step, the underrelaxation factor is reduced until a converged state of all transition points has been obtained.

The application of a boundary-layer method for the computation of all viscous data necessary for the transition prediction method ensures the high accuracy of the viscous data required by the e^N methods for the analysis of laminar boundary layers. Thus, as shown in [6], the large number of grid points near the wall for a high resolution of the boundary layers, the adaptation of the Navier–Stokes grid in the laminar, turbulent, and transitional boundary-layer regions and the generation of new adapted grids for the RANS solver after every step of the transition location iteration are avoided, and the computational time can be massively reduced. In addition, the number of RANS iteration cycles between two steps of the transition location iteration can be highly reduced compared to an approach where the boundary-layer parameters are computed directly from the RANS grid [23,24], because the surface pressure converges significantly faster in the RANS computation than the boundary-layer velocity profiles [25], which are the basis for the computation of the boundary-layer parameters.

The definition of a wing section is given by the boundary-layer edge streamlines running over the upper and lower sides of the wing originating in the boundary-layer edge point associated with the stagnation point (in 2-D problems) or attachment line point (in 3-D problems) on the wing surface in the area of the oncoming flow. At the moment, the FLOWer code is not yet capable to compute streamlines. Thus, a wing section is approximated by a surface grid line of the block-structured grid. The grid lines on the wing surface should be well parallel and more or less perpendicular to the leading and trailing edges of the wing.

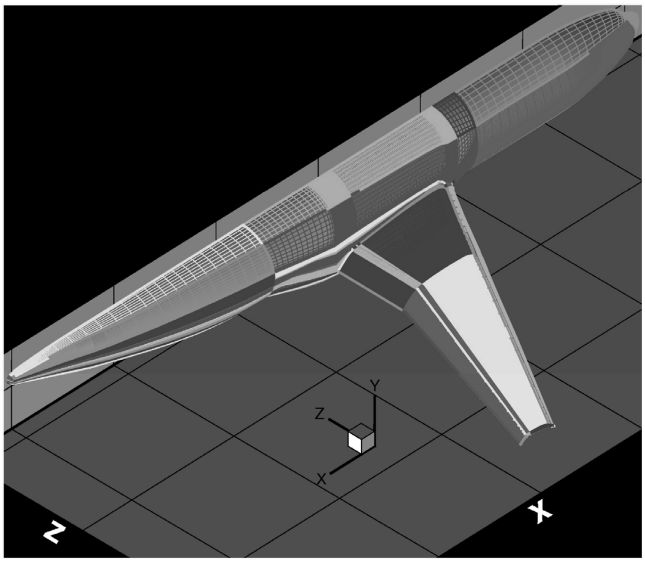

Fig. 2 Computational grid.

Details of the two e^N-database methods can be found in [8,9,20].

III. Computations

A. Test Cases

The first 3-D aircraft configuration the FLOWer code including the transition prediction module was applied to is based on the KH3Y geometry, also called DLR F11 model [26,27]. This wind-tunnel model is a half-model representing a modern transport aircraft with a fuselage of type Airbus A340 and a high-lift wing system that can be adjusted for different flight situations. The geometric configuration used in this work was the landing configuration of the F11 model with full span slat and flap defined in the European High-Lift Programme EUROLIFT [28]. The landing configuration exhibits a slat deflection angle of $\delta_S = 26.5$ deg and a flap deflection angle of $\delta_F = 32.0$ deg [26]. The model was experimentally tested during the EUROLIFT project in the Low Speed Wind Tunnel (LSWT) of Airbus Germany in Bremen. The aerodynamic configuration named TC214 refers to a freestream Reynolds number $Re_\infty = 1.35 \times 10^6$ (based on the reference chord length being the chord length of the wing in its retracted position at 39% of the half-span) and to a freestream Mach number $M_\infty = 0.174$. In the LSWT wind-tunnel experiments, transition was fixed on the fuselage 30 mm downstream of the fuselage nose tip.

The computations were carried out for two angles of attack, $\alpha = 10.0$ deg and $\alpha = 14.0$ deg, for fully turbulent flow, flow with prescribed transition locations, and flow with predicted transition locations. According to [29],[†] the transition locations for the computations with prescribed transition were imposed along the full span of all three wing elements as in Table 1. "Beneath main trailing edge" means that for the approximation of the real transition points on the flap upper side, those flap surface points were chosen that have the minimum distance to the upper-side trailing edge of the main wing element, which is located directly above the flap upper side. This approximation was chosen, because no indications for the flap upper-side transition locations are available from the experiments and because transition is very unlikely to occur upstream of that position because of the very highly accelerated flow in the channel between flap upper side and cove upper side of the main wing element.

In all cases, where numerical values were applied these values are based on the outcome of hot film measurements. Two hot films were placed on the slat and the main wing elements on the outboard wing at about 68% of the half-span of the wing.

In all computations with transition, transition was fixed at the fuselage nose according to the position of the tripping band in the experiment and "point transition" was applied; that is, no transition length models and no intermittency function were applied, but the flow domain was partitioned into pure laminar and pure turbulent portions with a discontinuous jump of an intermittency value $\gamma = 0$ in the fully laminar part to an intermittency value $\gamma = 1$ in the fully turbulent part.

The computational grid, Fig. 2, which was generated and provided by Airbus Germany, was a block-structured grid consisting of 97 blocks and approximately 5.51 million grid points and about 96.500 points on the surface of the geometry.

The computations were carried out using the Spalart–Allmaras one-equation model [30] with Edwards and Chandra modification

[†]Schrauf, G., "EUROLIFT II Task 1.2—On the Evaluation of the EUROLIFT LSWT Tests," Airbus Deutschland GmbH, Presentation Charts, Task 1.2&3.1 Technical Meeting in Toulouse, Dec. 2004.

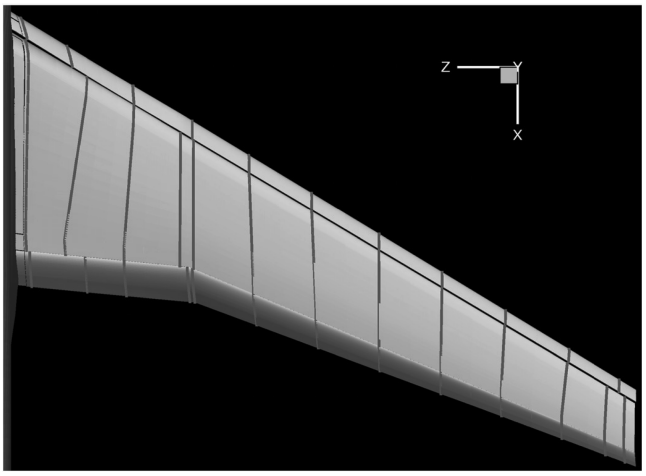

Fig. 3 Wings sections of all three wing elements (upper side) for which transition prediction was applied.

[31] (Spalart–Allmaras–Edwards = SAE), the cell-centered spatial discretization scheme, and low artificial dissipation settings $k^{(4)} = 1/64$ and $\zeta^{(\text{ratio EV})} = 0.1$, $\zeta^{(\text{ratio EV})}$ being the exponent of the eigenvalue ratios in the Martinelli coefficients.

B. Prescribed and Predicted Laminar Surface Regions

In the next figures, the prescribed and predicted laminar surface regions for the two test cases are shown. In the depictions, the different gray shades have the following meanings: Dark gray patches: surface cells whose four vertices are all laminar, that is, the intermittency value $\gamma = 0$ at all four vertices. Light gray patches: surface cells whose four vertices are not all laminar, that is, the intermittency value $\gamma = 1$ at one vertex at least. Dark lines: line that connects all vertices having the intermittency value $\gamma = 1$ at the border between fully laminar vertices ($\gamma = 0$) and fully turbulent vertices ($\gamma = 1$).

The stability analysis on the three elements of the wing was carried out in 11 sections on the slat, 13 sections on the main wing element, and 13 sections on the flap, which are represented by surface grid lines of the computational grid, Fig. 3.

The values for the critical N factors used for the e^N-database methods were defined in the following way: For $\alpha = 10.0$ deg, the hot film signals of the hot film placed on the main wing element at 68% of the half-span yielded a transition location of $(x^T/c)^{\text{main}} = 0.08$ on the upper side. In a test computation for $\alpha = 10.0$ deg in the corresponding wing section, only the e^N-database method for TS waves yielded amplified disturbances that were high enough such that transition could occur. The laminar separation point detected by the laminar boundary-layer code was located well downstream of the measured transition location $(x^T/c)^{\text{main}} = 0.08$. The e^N-database method for CF waves yielded highly damped disturbances, which were not high enough for transition to occur by a CF instability. According to the transition prediction tools available, only a TS instability could have led to transition in this section on the upper side of the main wing element.

The measured transition location $(x^T/c)^{\text{main}} = 0.08$ is reached for a critical N factor for TS waves of $N_{\text{crit}}^{\text{TS}} \approx 4.9$, which corresponds to a freestream turbulence level of $Tu_\infty \approx 0.4\%$ according to Mack's relationship, $N_{\text{crit}}^{\text{TS}} = -8.43 - 2.4\,\ell_n(Tu_\infty)$. Because there are no indications for the numerical value of the critical N factor for CF waves $N_{\text{crit}}^{\text{CF}}$, neither from the experiments, nor from the test computation, for $N_{\text{crit}}^{\text{CF}}$ the same numerical value as for $N_{\text{crit}}^{\text{TS}}$ is applied, $N_{\text{crit}}^{\text{CF}} = N_{\text{crit}}^{\text{TS}}$. Thus, for both critical N factors $N_{\text{crit}}^{\text{TS}} = N_{\text{crit}}^{\text{CF}} = 4.9$ is used.

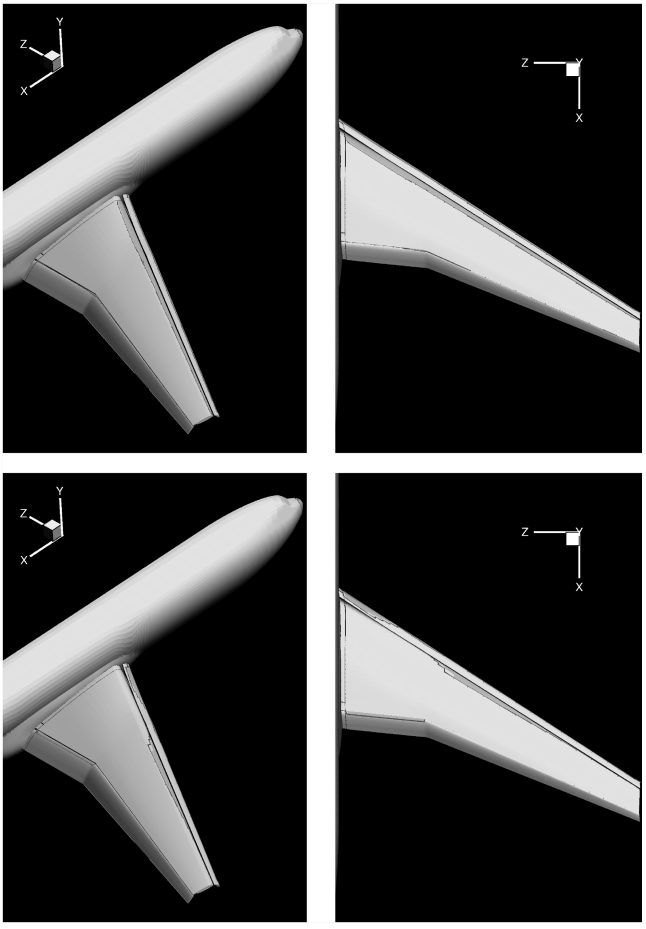

Fig. 4 Prescribed (above) and predicted (below) laminar surface regions on the upper side of the wing for the test case with $\alpha = 10.0$ deg.

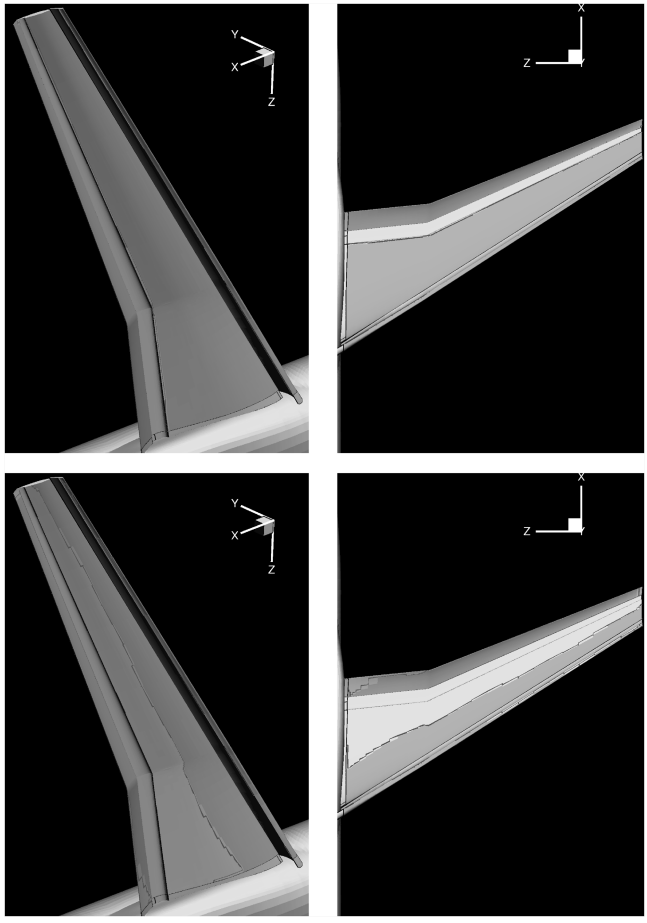

Fig. 5 Prescribed (above) and predicted (below) laminar surface regions on the lower side of the wing for the test case with $\alpha = 10.0$ deg.

The computational results of the RANS solution process were considered converged when the following criteria were satisfied: 1) the global normalized density residual had decreased by three orders of magnitude, and 2) for the lift coefficient c_L the threshold value $\varepsilon(c_L) = (c_L - c_{L,\text{end}})/c_{L,\text{end}}$ satisfies the condition $|\varepsilon(c_L)| < 0.001$ for the last 100 iteration cycles of the RANS computation. The transition location iteration procedure was stopped for a single transition location when the absolute difference between two consecutive transition point values was lower than 5%. For all the results presented in this publication, these convergence criteria were satisfied.

In Fig. 4, the prescribed and predicted laminar surface regions for the test case with $\alpha = 10.0$ deg are shown for the upper side, in Fig. 5 for the lower side.

In Fig. 6, the prescribed and predicted laminar surface regions for the test case with $\alpha = 14.0$ deg are shown for the upper side, in Fig. 7 for the lower side.

In Figs. 8 and 9, the predicted laminar surface regions for the two different test cases are compared. The wing sections, in which the transition locations were predicted, are marked. Each section of each wing element is labeled according to the transition mechanism which led to transition when transition occurred due to a TS instability or due to a CF instability. When there is no label at the wing element section, either the transition point was approximated by a laminar separation point from the laminar boundary-layer code, because no amplified disturbances exceeding the two critical N factors were found by the two e^N-database methods upstream of that point where the laminar boundary layer separates, or transition did not occur at all; that is, neither the e^N-database methods detected an instability nor the boundary-layer code found a laminar separation upstream of the trailing edge. On the lower side of the wing, the flow remained laminar up to the trailing edge in the sections 1–6 (section 1 is the innermost section at the wing root) of the slat and in the sections 5–13 of the flap for $\alpha = 10.0$ deg and in the sections 1–5 of the slat and in the sections 5–13 of the flap for $\alpha = 14.0$ deg. The transition lines on the lower sides of the slat and the main wing element for the two test cases are very similar to each other but they are not identical, whereas the transition lines on the flap lower side are identical for both test cases. In Fig. 8, the results for the upper side are compared, in Fig. 9 for the lower side.

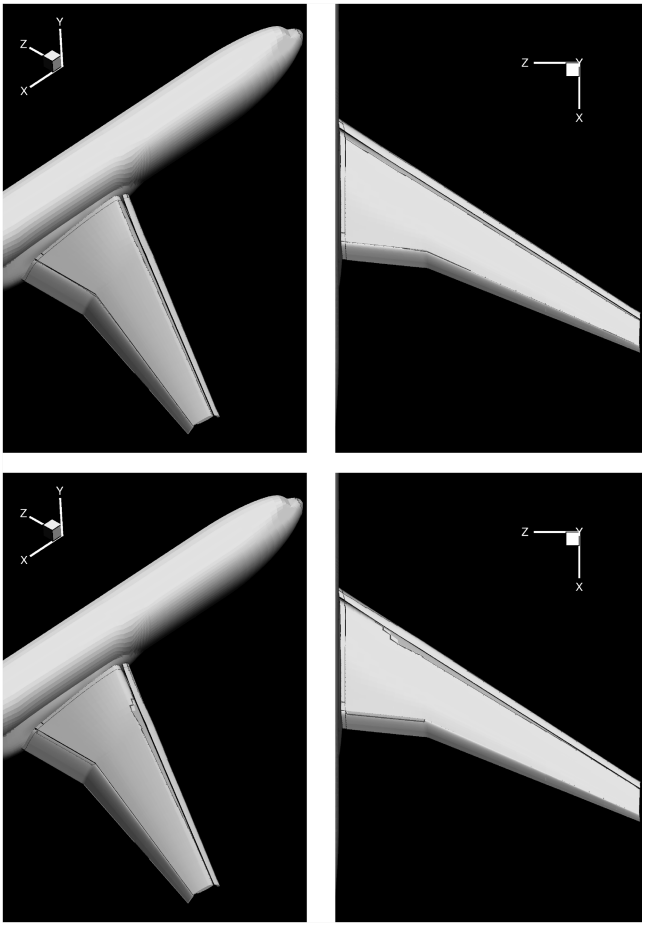

Fig. 6 Prescribed (above) and predicted (below) laminar surface regions on the upper side of the wing for the test case with $\alpha = 14.0$ deg.

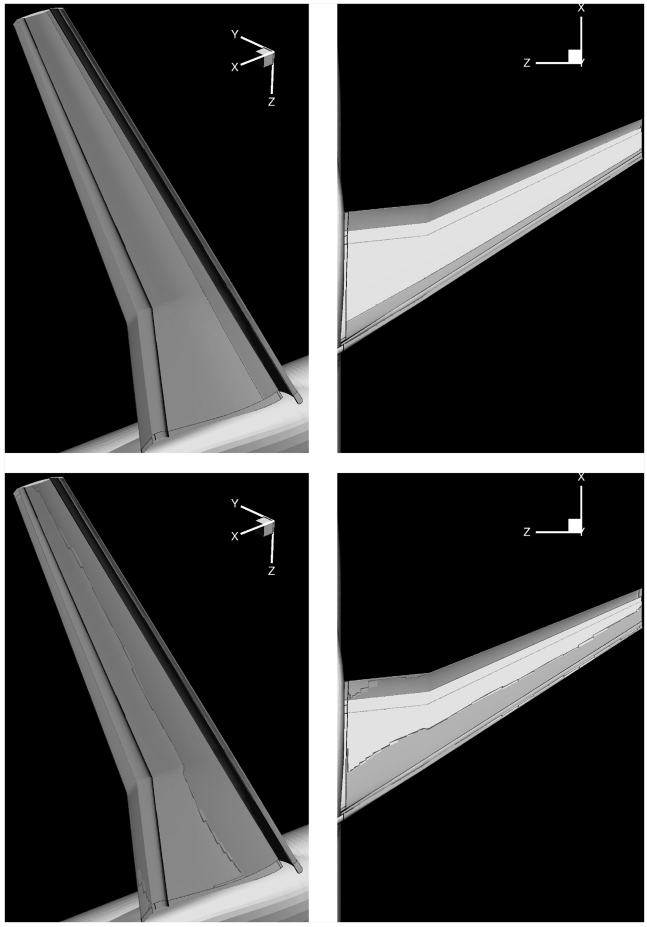

Fig. 7 Prescribed (above) and predicted (below) laminar surface regions on the lower side of the wing for the test case with $\alpha = 14.0$ deg.

Along wide portions of the span, the boundary-layer code predicts laminar separation on the upper side of the wing very closely downstream of the nose of the slat, for the sections 6–13 for $\alpha = 10.0$ deg and for the sections 4–13 for $\alpha = 14.0$ deg. The same situation occurs on the main wing element in the sections 1–5 and 11–13 for $\alpha = 10.0$ deg and for the sections 1–2 and 11–13 for $\alpha = 14.0$ deg. On the flap, the whole upper side of the outboard wing beyond the kink is fully turbulent in both test cases because according to the boundary-layer code the laminar boundary layer separates directly at the nose points of the wing sections, that is, in the sections 5–13.

The next figures compare the transition lines in the area where the hot films were placed in the experiment. The upper picture in Fig. 10 compares the prescribed transition lines (medium gray lines) and the predicted transition lines (dark gray lines) for $\alpha = 10.0$ deg. The two lines drawn across the main wing only mark the wing sections used for the transition prediction on the left-hand side and right-hand side of the hot film position. The wing section on the left-hand side of the hot film position was used for the calibration of the critical N factor for TS instabilities. The predicted transition location on the main wing upper side in the wing section of the hot film position is well reproduced; the predicted transition location on the slat upper side is located slightly upstream of that given by the hot film. The lower picture in Fig. 10 compares the prescribed transition lines (medium gray lines) and the predicted transition lines (dark gray lines) for $\alpha = 14.0$ deg. Both transition locations, on the main wing upper

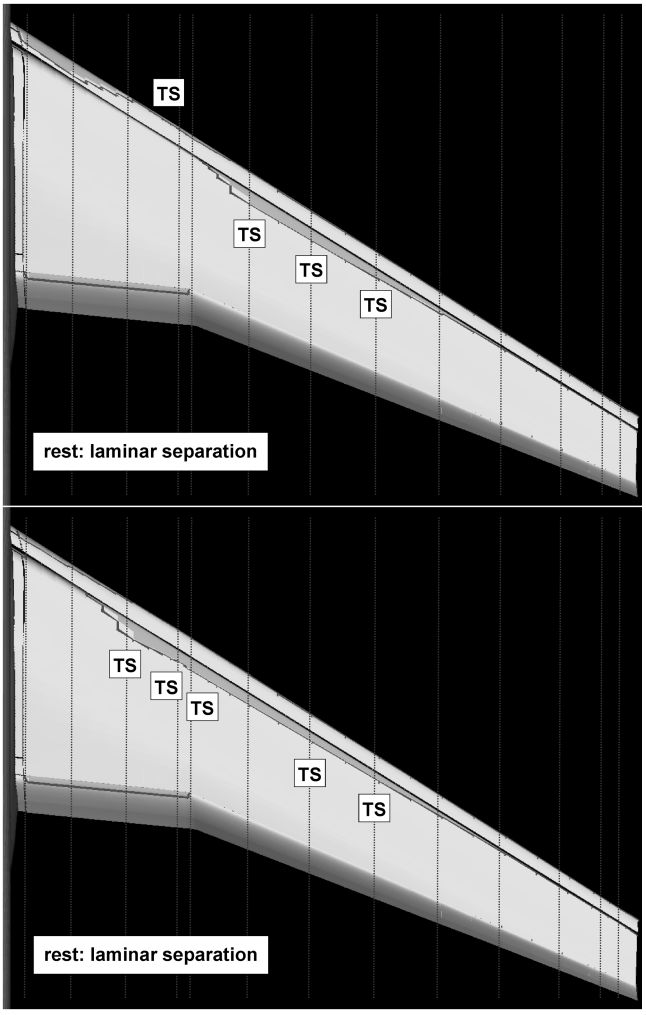

Fig. 8 Predicted laminar surface regions, upper side, for $\alpha = 10.0$ deg (above) and $\alpha = 14.0$ deg (below) and sections in which transition prediction was performed with transition mechanism labels.

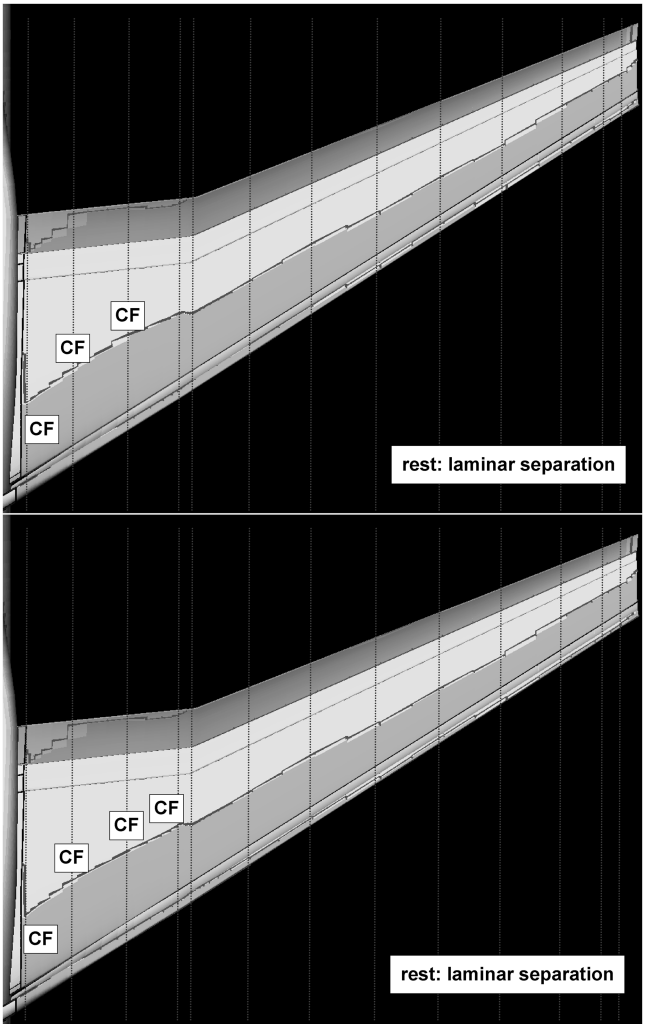

Fig. 9 Predicted laminar surface regions, lower side, for $\alpha = 10.0$ deg (above) and $\alpha = 14.0$ deg (below) and sections in which transition prediction was performed with transition mechanism labels.

side and on the slat upper side, are well reproduced although the slat upper-side transition location is located very slightly upstream of that given by the hot film.

C. Pressure Distributions

In the following, a comparison of the computed and measured c_p distributions in four wing sections at the spanwise stations $\eta = z/b = 0.205$, 0.385, 0.662, and 0.878 are presented, for $\alpha = 10$ deg in Fig. 11 and for $\alpha = 14$ deg in Fig. 12. Here, b is the length of the half-span and z is the value of the coordinate pointing in spanwise direction and being perpendicular to the longitudinal axis (x direction) of the configuration. Both values are measured from the symmetry plane of the configuration.

For both angles of attack, the expected impact of taking into account transition can be found. The pressure levels in the results from the computations with transition are lowered to more negative values in all wing sections for both test cases compared to the pressure levels of fully turbulent flow. This finding applies for the complete chord length of each wing element in each wing section except for section 4 in the flow case with prescribed transition, and is pronounced in the regions of the suction peaks and near the trailing edge of the main wing element. The agreement of the computed and measured c_p distributions is good for the flow cases with fully turbulent flow and with predicted transition. A clearly visible improvement was achieved for the test case with $\alpha = 14.0$ deg for the flow case with predicted transition. Here, the computed c_p distributions now match the measured values in the area of the suction peaks of the main wing element and of the flap in the wing sections 2 and 3. Along the flap upper side, the pressure levels are shifted into the direction of the measured ones in the wing sections 1, 2, and 3. The same effect can be observed in the wing sections 2 and 3 on the main wing element in the area between 50 and 100% of the local chord lengths.

The results of the computations with prescribed transition that show almost the same c_p distributions in the wing sections 1, 2, and 3 as the results from the flow case with predicted transition suffer from strong deficiencies in section 4 for both test cases. For $\alpha = 10.0$ deg, the c_p distribution on the flap upper side deviates strongly from the measured one at about 45% of the local chord length, indicating a trailing-edge separation. The existence of the pressure plateau is an indication for a bubblelike separation with relatively large components of reverse flow. Presumably, this type of separation did not exist in the flow during the experiment. If separation occurred at all, it must have been rather of spanwise-flow type, exhibiting large components of flow in spanwise direction and only small components of reverse flow. The strong trailing-edge separation influences the flap upper-side suction peak, which is lower than that of the flow cases with fully turbulent flow and predicted transition, and it also has an influence on the pressure level on the main wing trailing edge. In the test case with $\alpha = 14.0$ deg, the flap separation starts directly downstream of the leading edge. The flow over the flap upper side is completely detached in this area with strong reverse flow components. Here, the influence on the circulation is so strong that the pressure levels on the flap lower side and on the upper side of the main wing element up to 40% of the local chord length are both heavily affected. Apart from effects coming from the turbulence model used (it is possible that shortcomings of the turbulence model

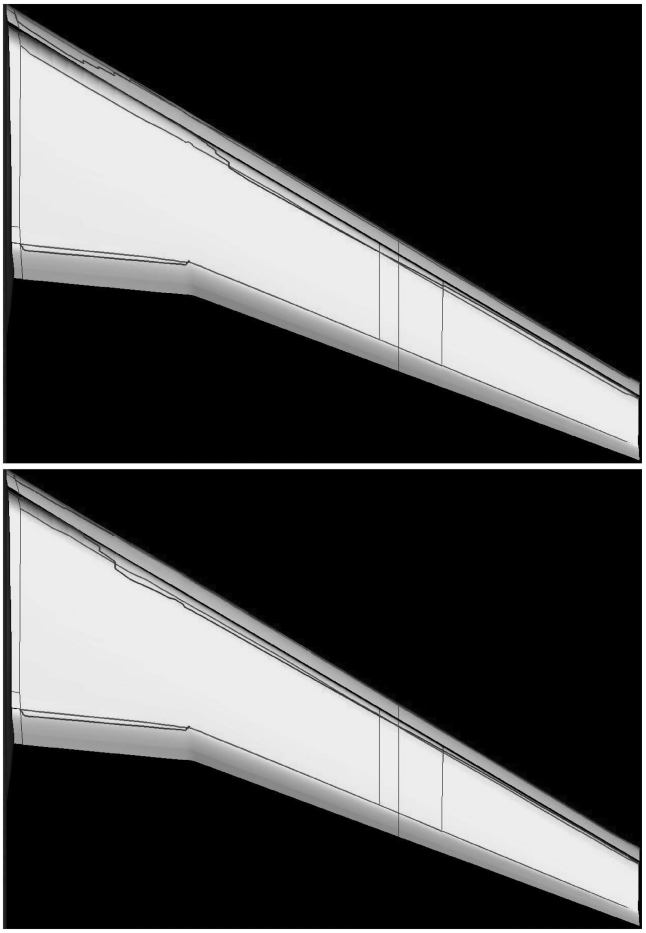

Fig. 10 Prescribed and predicted transition lines for $\alpha = 10.0$ deg (above) and $\alpha = 14.0$ deg (below).

contribute to this deficiency) these errors in the separation strength near the wing tip can be an indication that the laminar regions in this area that increase the tendency for separation were overestimated in the flow case with prescribed transition.

A further assessment of the results obtained requires a comparison of other experimentally measured parameters such as global force coefficients or a comparison of, for example, the surface skin friction lines with flow visualizations on the one hand. On the other hand, it would be highly appreciated if more transition data were available to validate the transition prediction methods and tools and to justify their application to complex configurations as well as possible.

IV. Conclusions

A Reynolds-averaged Navier–Stokes solver with transition prediction capabilities was successfully applied to an industrially relevant wing-body high-lift aircraft configuration with a three-element wing consisting of a main wing with full span slat and flap. The RANS solver, which is coupled to a transition prediction module, represents a simulation system that predicts the unknown transition locations during the ongoing RANS computation iteratively in an automatic manner without intervention of the user of the code. The transition prediction module consists of a laminar boundary-layer method for swept, tapered wings and compressible, conical external flow and of two e^N-database methods for Tollmien–Schlichting and crossflow instabilities.

The computations were carried out for two angles of attack, $\alpha = 10.0$ deg and $\alpha = 14.0$ deg, for three different flow cases: fully turbulent, with prescribed transition lines, and with predicted transition lines. It was shown that the results from the computations with predicted transition lines yield c_p distributions, which show a better agreement with experimental ones than in a comparison with fully turbulent results on the one hand. On the other hand, it was found that in the computations with prescribed transition lines, some flow features were not correctly reproduced. Because the laminar regions were overestimated in some areas of the flowfield, the separation behavior in these regions turned out to be of erroneous character and strength.

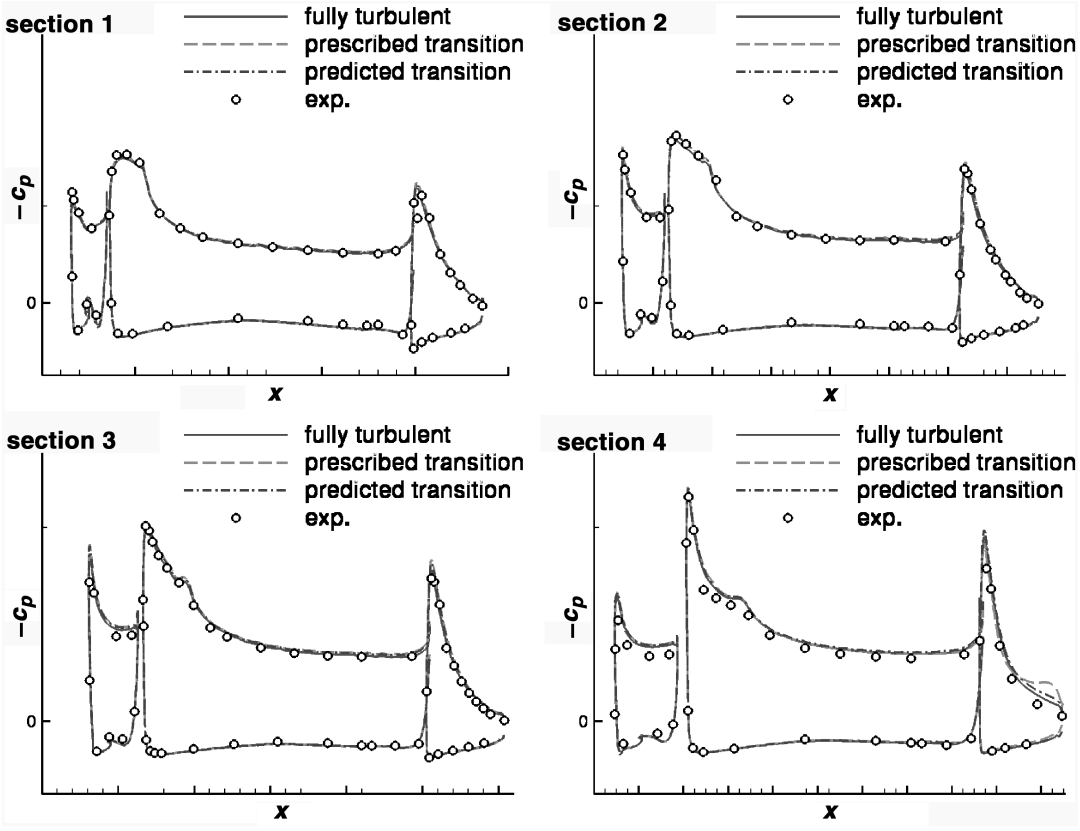

Fig. 11 Computed and measured c_p distributions at $\eta = 0.205$, 0.385, 0.662, and 0.878 for $\alpha = 10.0$ deg.

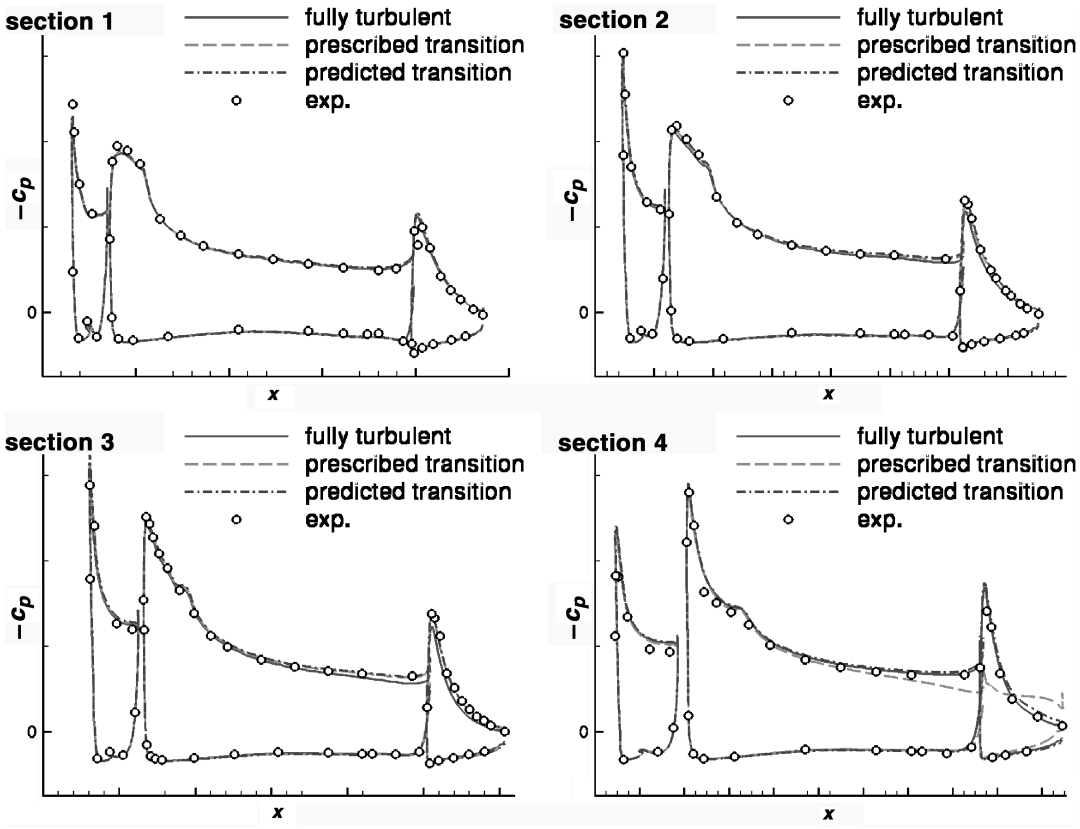

Fig. 12 Computed and measured c_p distributions at $\eta = 0.205, 0.385, 0.662$, and 0.878 for $\alpha = 14.0$ deg.

Finally, it must be emphasized that with the current version of the transition prediction module, typical transition mechanisms that can occur in 3-D high-lift flows are not yet covered, for example, attachment line transition or bypass transition in boundary layers, which are affected by the wake of an upstream located wing element. Moreover, the approximation of transition points inside laminar separation bubbles using the laminar separation points from a laminar boundary-layer code can be questioned. Therefore, an extension of the transition prediction module by the incorporation of criteria for these transition mechanisms is indispensable. In this sense, the results presented are of preliminary character with regard to the conclusiveness of the predicted transition locations. The main objective, however, which was to demonstrate that the underlying transition prediction procedure embedded in the RANS code FLOWer is capable of being applied to complex aircraft configurations of industrial relevance, was achieved.

Acknowledgments

This work has been carried out within the EUROLIFT II project (European High-Lift Programme II) [32]. The EUROLIFT II project is a collaboration between German Aerospace Center (DLR), Airbus-Deutschland, Airbus-France, Airbus-United Kingdom, Alenia Aeronautica S.p.A, ICAROS Computing Ltd., Dassault Aviation, Centro Italiano Ricerche Aerospaziali S.C.p.A. (CIRA), European Transonic Wind Tunnel GmbH (ETW), IBK Ingenieurbüro Dr. Kretschmar, Instituto Nacional de Tecnica Aeroespacial (INTA), Office National d'Études et de Recherches Aérospatiale (ONERA), Stichting Nationaal Lucht- en Ruimtevaart Laboratorium (NLR), and the Swedish Defense Research Agency (FOI). The project is managed by DLR and is partly funded by the European Union (Project Ref: GRD-2004-502896).

References

[1] Rudnik, R., Ronzheimer, A., and Schenk, M., "Berechnung von zwei- und dreidimensionalen Hochauftriebskonfigurationen durch Lösung der Navier-Stokes Gleichungen," *Deutschen Gesellschaft für Luft- und Raumfahrt (DGLR), JT 96-104, Deutscher Luft- und Raumfahrtkongreß, DGLR-Jahrestagung*, Deutsche Gesellschaft für Luft- und Raumfahrt, Lilienthal-Oberth, DGLR, D-53175 Bonn, Germany, 1996, pp. 717–726.

[2] Smith, A. M. O., and Gamberoni, N., "Transition, Pressure Gradient and Stability Theory," Douglas Aircraft Company, Rept. ES 26388, Long Beach, CA, 1956.

[3] van Ingen, J. L., "A Suggested Semi-Empirical Method for the Calculation of the Boundary Layer Transition Region," Univ. of Delft, Rept. VTH-74, Dept. of Aerospace Engineering, Delft, The Netherlands, 1956.

[4] Arnal, D., and Casalis, G., "Laminar-Turbulent Transition Prediction in Three-Dimensional Flows," *Progress in Aerospace Sciences*, Vol. 36, 2000, pp. 173–191.

[5] Radespiel, R., Graage, K., and Brodersen, O., "Transition Predictions Using Reynolds-Averaged Navier-Stokes and Linear Stability Analysis Methods," AIAA Paper 91-1641, 1991.

[6] Stock, H. W., and Haase, W., "A Feasibility Study of e^N Transition Prediction in Navier-Stokes Methods for Airfoils," *AIAA Journal*, Vol. 37, No. 10, 1999, pp. 1187–1196.

[7] Horton, H. P., and Stock, H. W., "Computation of Compressible, Laminar Boundary Layers on Swept, Tapered Wings," *Journal of Aircraft*, Vol. 32, No. 6, 1995, pp. 1402–1405.

[8] Stock, H. W., and Degenhardt, E., "A Simplified e^N Method for Transition Prediction in Two-Dimensional, Incompressible Boundary Layers," *Zeitung für Flugwissenschaft und Weltraumforschung*, Vol. 13, 1989, pp. 16–30.

[9] Casalis, G., and Arnal, D., "ELFIN II Subtask 2.3: Database Method—Development and Validation of the Simplified Method for Pure Crossflow Instability at Low Speed," ELFIN II—European Laminar Flow Investigation, Technical Report no. 145, ONERA-CERT, R.T. DERAT no. 119/5618.16, Département d'Études et de Recherches en Aérothermodynamique (DERAT), Dec. 1996.

[10] Crouch, J. D., Crouch, I. W. M., and Ng, L. L., "Transition Prediction for Three-Dimensional Boundary Layers in Computational Fluid Dynamics Applications," *AIAA Journal*, Vol. 40, No. 8, 2002, pp. 1536–1541.

[11] Warren, E. S., and Hassan, H. A., "Transition Closure Model for Predicting Transition Onset," *Journal of Aircraft*, Vol. 35, No. 5, 1998, pp. 769–775.

[12] Czerwiec, R. M., Edwards, J. R., Rumsey, C. L., Bertelrud, A., and Hassan, H. A., "Study of High-Lift Configurations Using k-ζ

Transition/Turbulence Model," AIAA Paper 99-3186, 1999.
[13] Edwards, J. R., Roy, C. J., Blottner, F. G., and Hassan, H. A., "Development of a One-Equation Transition/Turbulence Model," *AIAA Journal*, Vol. 39, No. 9, 2001, pp. 1691–1698.
[14] Langtry, R. B., and Menter, F. R., "Transition Modeling for General CFD Applications in Aeronautics," AIAA Paper 2004-522, 2005.
[15] FLOWer - Installation and User Handbook, Release 116, Doc.Nr. MEGAFLOW-1001, Institut für Entwurfsaerodynamik, Deutsches Zentrum für Luft- und Raumfahrt, e. V., Göttingen, Germany, 2000.
[16] Krumbein, A., and Stock, H. W., "Laminar-Turbulent Transition Modeling in Navier-Stokes Solvers Using Engineering Methods," *ECCOMAS 2000* [CD-ROM], International Center for Numerical Methods in Engineering (CIMNE), 2000, Depósito Legal: B-37139-2000.
[17] Krumbein, A., "Coupling of the DLR Navier-Stokes Solver FLOWer with an e^N-Database Method for Laminar-Turbulent Transition Prediction on Airfoils," *New Results in Numerical and Experimental Fluid Mechanics III*, Vol. 77, Notes on Numerical Fluid Mechanics, Springer–Verlag, Berlin, 2002, pp. 92–99.
[18] Krumbein, A., "Transitional Flow Modeling and Application to High-Lift Multi-Element Airfoil Configurations," *Journal of Aircraft*, Vol. 40, No. 4, 2003, pp. 786–794.
[19] Krumbein, A., "Automatic Transition Prediction and Application to Three-Dimensional Wing Configurations," *Journal of Aircraft*, Vol. 44, No. 1, 2007, pp. 119–133; also AIAA Paper 2006-914, June 2006.
[20] Krumbein, A., "Automatic Transition Prediction and Application to High-Lift Multi-Element Configurations," *Journal of Aircraft*, Vol. 42, No. 5, 2005, pp. 1150–1164; also AIAA Paper 2004-2543, June–July 2004.
[21] Jameson, A., Schmidt, W., and Turkel, E., "Numerical Solutions of the Euler Equations by Finite-Volume Methods Using Runge-Kutta Time-Stepping Schemes," AIAA Paper 81-1259, 1981.
[22] Martinelli, L., and Jameson, A., "Validation of a Multigrid Method for the Reynolds-Averaged Navier-Stokes Equation," AIAA Paper 88-0414, 1988.
[23] Krumbein, A., "Navier-Stokes Airfoil Computations with Automatic Transition Prediction Using the DLR TAU Code—A Sensitivity Study," *New Results in Numerical and Experimental Fluid Mechanics V*, Vol. 92, Notes on Numerical Fluid Mechanics and Multidisciplinary Design, Springer–Verlag, Berlin, 2006, pp. 192–199.
[24] Krumbein, A., "Automatic Transition Prediction for High-Lift Systems Using a Hybrid Flow Solver," *Journal of Aircraft*, Vol. 42, No. 5, 2005, pp. 1362–1366.
[25] Nebel, C., Radespiel, R., and Wolf, T., "Transition Prediction for 3D Flows Using a Reynolds-Averaged Navier-Stokes Code and N-Factor Methods," AIAA Paper 2003-3593, 2003.
[26] Puffert-Meißner, W., "The DLR F11 (KH3Y) Model Configurations used in the EUROLIFT Programme," DLR, Technical Report IB 124-2004/9, Braunschweig, Germany, March 2004.
[27] Rudnik, R., "Description of Test Case 214," EUROLIFT, DLR, Technical Note EL-TN-2.1.2-1, Braunschweig, Germany, Sep. 2004.
[28] EUROLIFT - European High-Lift Programme, "Description of Work," GROWTH Project, GRD1-1999-10015, 1999.
[29] Perraud, J., "Minutes of Task 1.2&3.1 Meeting in Toulouse," ONERA, CM ELII-ONERA-12-004, Toulouse, France, January 2005.
[30] Spalart, P. R., and Allmaras, S. R., "A One-Equation Turbulence Model for Aerodynamic Flows," *La Recherche Aérospatiale*, No. 1, 1994, pp. 5–21.
[31] Edwards, J. R., and Chandra, S., "Comparison of Eddy Viscosity–Transport Turbulence Models for Three-Dimensional, Shock-Separated Flowfields," *AIAA Journal*, Vol. 34, No. 4, 1996, pp. 756–763.
[32] EUROLIFT II-European High-Lift Programme II, Annex B, "Description of Work," 6th European Framework Program, Research Project, GRD-2004-502896, 2004.